Atmos. Chem. Phys., 12, 8813–8828, 2012
www.atmos-chem-phys.net/12/8813/2012/
doi:10.5194/acp-12-8813-2012

Atmospheric Chemistry and Physics

On the dependence of the OH* Meinel emission altitude on vibrational level: SCIAMACHY observations and model simulations

C. von Savigny[1], **I. C. McDade**[2], **K.-U. Eichmann**[3], **and J. P. Burrows**[3]

[1]Institute of Physics, Ernst-Moritz-Arndt University of Greifswald, Greifswald, Germany
[2]Centre for Research in Earth and Space Science (CRESS) and Department of Earth and Space Science and Engineering (ESSE), York University, Toronto, Ontario, Canada
[3]Institute of Environmental Physics, University of Bremen, Bremen, Germany

Correspondence to: C. von Savigny (csavigny@physik.uni-greifswald.de)

Received: 15 January 2012 – Published in Atmos. Chem. Phys. Discuss.: 23 February 2012
Revised: 31 July 2012 – Accepted: 16 September 2012 – Published: 28 September 2012

Abstract. Measurements of the OH Meinel emissions in the terrestrial nightglow are one of the standard ground-based techniques to retrieve upper mesospheric temperatures. It is often assumed that the emission peak altitudes are not strongly dependent on the vibrational level, although this assumption is not based on convincing experimental evidence. In this study we use Envisat/SCIAMACHY (Scanning Imaging Absorption spectroMeter for Atmospheric CHartographY) observations in the near-IR spectral range to retrieve vertical volume emission rate profiles of the OH(3-1), OH(6-2) and OH(8-3) Meinel bands in order to investigate whether systematic differences in emission peak altitudes can be observed between the different OH Meinel bands. The results indicate that the emission peak altitudes are different for the different vibrational levels, with bands originating from higher vibrational levels having higher emission peak altitudes. It is shown that this finding is consistent with the majority of the previously published results. The SCIAMACHY observations yield differences in emission peak altitudes of up to about 4 km between the OH(3-1) and the OH(8-3) band.

The observations are complemented by model simulations of the fractional population of the different vibrational levels and of the vibrational level dependence of the emission peak altitude. The model simulations reproduce the observed vibrational level dependence of the emission peak altitude well – both qualitatively and quantitatively – if quenching by atomic oxygen as well as multi-quantum collisional relaxation by O_2 is considered. If a linear relationship between emission peak altitude and vibrational level is assumed, then a peak altitude difference of roughly 0.5 km per vibrational level is inferred from both the SCIAMACHY observations and the model simulations.

1 Introduction

It is generally assumed that the exothermic reaction of H and O_3,

$$H + O_3 \longrightarrow OH(v' \leq 9) + O_2 \quad \text{(R1)}$$

is the main source of vibrationally excited OH near the mesopause, producing an emission layer – first identified by Meinel (1950) – that is centered at about 87 km with a full width at half maximum (FWHM) of about 8–10 km (e.g. Baker and Stair, 1988). The first observation of the OH emission peak altitude was carried out in 1956 at the White Sands Proving Ground (New Mexico, US) using rocket photometer observations of the OH(9-3) band (Heppner and Meredith, 1958).

Ground-based observations of different OH Meinel bands are among the standard techniques to remotely sense the temperature of the emitting layer (e.g. French and Mulligan, 2010; Sigernes et al., 2003; Bittner et al., 2002; Espy and Stegman, 2002; Reisin and Scheer, 2002). If simultaneous observations of the vertical volume emission rate profile of the OH band analyzed are not available, the interpretation of the temperature retrievals may be difficult. An extreme example is the dramatic decrease of the OH emission layer altitude down to about 78 km observed in early 2004 at high northern latitudes, leading to an apparent temperature increase of

about 15 K (Dyrland et al., 2010). Long-term, solar cycle and seasonal variations in OH emission altitude can also lead to apparent variations in ground-based OH temperature measurements, and may interfere with the determination of the actual long-term, solar cycle and seasonal variations of upper mesospheric temperatures.

Previous studies showed characteristic variations of the OH emission altitude with latitude (Marsh et al., 2006; Baker et al., 2007), time of the year (e.g., Baker et al., 2007), longitude (e.g., Liu and Shepherd, 2006) and with solar activity (Liu and Shepherd, 2006). On shorter time scales, the height of the OH emission layer is affected by characteristic tidal variations (Ward, 1999) with maximum changes of about 3 km during the course of the night (e.g., Yee et al., 1997).

Another potential difficulty for the interpretation of ground-based OH rotational temperature measurements is related to the possibility that Meinel bands originating from different vibrational levels may have different peak emission altitudes. The number of previous studies dealing with this aspect is rather limited. Furthermore, the main results of these studies are partly contradictory. Some model (McDade, 1991) and experimental studies (Mende et al., 1993) indicate that differences in emission peak altitudes for different vibrational levels are rather small. Other model (Makhlouf et al., 1995; Adler-Golden, 1997; Baker and Stair, 1988; Xu et al., 2012) and experimental results (Kaufmann et al., 2008; Xu et al., 2012) suggest a vibrational level dependence of the emission peak altitude of several km. Xu et al. (2012) recently provided a comparison of SABER OH emission observations and model results that showed evidence for a vibrational level dependence of the OH emission altitude with emissions from higher vibrational levels occurring at higher altitudes.

In this context it is also relevant to mention that according to Cosby and Slanger (2007) significant changes in the relative population of the OH vibrational levels occur throughout the night. Furthermore, the magnitude of these nocturnal variations changes from night to night. The OH vibrational population has to be considered a dynamic equilibrium between OH* production preferably in the higher vibrational levels ($\nu' = 7, 8, 9$) and collisional as well as radiative transfer to lower vibrational levels (Cosby and Slanger, 2007).

In this study we use nightglow observations with SCIAMACHY on Envisat to retrieve vertical volume emission rate profiles of the OH(3-1), OH(6-2) and the OH(8-3) Meinel bands, in order to investigate whether systematic differences exist in the mean emission altitudes of these bands. The three bands were chosen because they are the most commonly used bands for ground-based OH temperature retrievals. The SCIAMACHY observations are complemented by model simulations using an extended version of the model by McDade (1991).

The paper is structured as follows. Section 2 provides information on the SCIAMACHY instrument and the Envisat satellite. The inversion method employed for the retrieval of vertical emission rate profiles from limb emission profiles is described in Sect. 3. The inversion results together with a discussion are presented in Sect. 4. In Sect. 5 the modelled OH(ν) fractional populations and volume emission rate profiles for different vibrational levels are presented and discussed. Section 6 briefly discusses the implications of the differences in emission peak altitude for different vibrational levels for measurements of OH rotational temperatures from the ground. Conclusions are provided at the end.

2 SCIAMACHY on Envisat

SCIAMACHY, the Scanning Imaging Absorption spectroMeter for Atmospheric CHartrographY (Burrows et al., 1995; Bovensmann et al., 1999) on ESA's Envisat is an 8-channel grating spectrograph covering the spectral range from about 214 nm up to about 2380 nm. Envisat was launched on 1 March 2002 into a sun-synchronous polar orbit with an inclination of 98.55° and a descending node at 10:00 a.m. local solar time. SCIAMACHY observes scattered, reflected, transmitted and emitted electromagnetic radiation in nadir, solar/lunar occultation and limb-viewing geometry. Unfortunately, SCIAMACHY measurements abruptly ceased on 8 April 2012 with a fatal spacecraft failure. The main focus of the SCIAMACHY limb observations is on the daytime measurements of scattered solar radiation allowing, e.g. retrievals of stratospheric O_3, NO_2 and BrO profiles as well as stratospheric aerosol extinction profiles. However, SCIAMACHY also performs limb observations on the Earth's night-side covering the tangent height range from about 72 km up to 150 km. These night-time or ecplise limb observations are employed in the current study. Note, that the local time of all SCIAMACHY measurements used for this study is close to 10:00 p.m. The eclipse limb measurements are also used to retrieve OH rotational temperatures from the OH(3-1) Meinel band (von Savigny et al., 2004). Unfortunately, these measurements do not cover the entire latitude range on the dark side of the Earth, because blocks of limb measurements are interrupted by calibration measurements. The range of latitudes covered changes with season, such that, e.g. high northern latitudes are only observed during northern winter. Continuous coverage throughout the year is only possible between about 10° S and 20° N. The vertical field of view of the limb observations is about 2.6–2.8 km at the tangent point, and the limb spectra are recorded in tangent height steps of 3.3 km.

During the early phases of the SCIAMACHY mission the limb tangent height information was affected by errors of up to several km (Kaiser et al., 2004; von Savigny et al., 2005). The main reasons for these tangent height errors – satellite attitude knowledge errors as well as a misalignment between the SCIAMACHY optical axes and the satellite reference frame – were identified and corrected (Gottwald et al., 2007).

Only the most recent SCIAMACHY Level 1 data versions (7.03 and 7.04) are used in this study including the most up-to-date corrections for instrument misalignments and satellite attitude errors. Recent investigations of potential anomalous drifts in SCIAMACHY tangent height information using solar occultation observations indicate tangent height trends of less than about 20 m yr^{-1} (Bramstedt et al., 2012). These small trends in the limb tangent height information render the SCIAMACHY data set suitable to study possible temporal variations in the altitude of the OH Meinel emission layer. Calibration of the SCIAMACHY raw data (Level 1b data) was performed without correction for the memory effect and polarization (calibration flags 0 and 6), due to known problems with these corrections.

3 Methodology: inversion of volume emission rate profiles

SCIAMACHY provides measurements of the limb emission rates integrated along the tangent line of sight. These limb emission rates (being a function of tangent height) have to be inverted to vertical volume emission rate profiles (as a function of geometrical altitude). The inversion was performed with a regularized least squares technique with statistical weighting. The retrieval altitude grid was chosen to be identical with the tangent height grid of the limb observations, i.e. the spacing between adjacent altitude levels is about 3.3 km. The retrieval is based on the assumption that the hydroxyl layer can be approximated by a set of 10 homogeneously emitting layers of 3.3 km thickness with center altitudes ranging from about 73 km up to 103 km.

The basic inversion equation is given by:

$$\boldsymbol{x} = \left(\mathbf{K}^T\mathbf{S}^{-1}\mathbf{K} + \gamma\mathbf{R}^T\mathbf{R}\right)^{-1}\mathbf{S}^{-1}\mathbf{K}^T\boldsymbol{y} \quad (1)$$

Here, $\boldsymbol{x} = [x_1, x_2, \ldots, x_M]^T$ corresponds to the retrieved solution of the vertical emission rate profile, and $\boldsymbol{y} = [y_1, y_2, \ldots, y_N]^T$ corresponds to the measured limb emission profile (spectrally averaged over wavelength ranges presented in Table 1). The elements K_{ij} of the matrix $\mathbf{K}$ are geometric weighting factors corresponding to the length of the transect of limb line of sight i through layer j of the model atmosphere. In the present case M equals N (i.e. $\mathbf{K}$ is a square matrix) because the retrieval altitude grid is identical to the tangent height grid. $\mathbf{S}$ is the measurement covariance matrix and is assumed to be diagonal. $\mathbf{R}$ and γ are the regularization matrix and the regularization parameter, respectively, and the standard $\mathbf{L}_1$ matrix was chosen as regularization matrix.

Table 1. Spectral windows used for the different OH Meinel bands.

OH band	Spectral interval
3-1	1515–1546 nm
6-2	837.5–848 nm
8-3	730–738 nm

The regularization parameter γ was iteratively adjusted until χ^2 – as defined in the following equation – is identical to the summed up variances of the limb-radiances:

$$\chi^2 = \sum_{i=1}^{N}\left(\sum_{j=1}^{M} K_{ij}x_j - y_i\right)^2 \approx \sum_{i=1}^{N}\sigma_{y_i}^2 \quad (2)$$

Because single OH(8-3) spectra ($\Delta\nu = 5$) as observed with SCIAMACHY are characterized by low signal-to-noise ratios, we determined monthly and zonally averaged limb spectra for 10° latitude bins (Fig. 1 shows some sample spectra). This is possible, because the tangent heights associated with the different tangent height steps are essentially identical for different limb measurements, at least within a month. We note that zonal averaging will eliminate the potentially significant longitudinal variations in OH Meinel emissions reported in earlier studies (e.g. Baker et al., 2007; Gao et al., 2011).

The monthly averaged limb measurements consist of averaged limb spectra for the different tangent heights ranging from about 72 km to about 110 km. An additional radiance offset correction was performed by subtracting the average of the 2 spectra at tangent height steps 11 and 12 (about 107 km and 110 km) from the limb spectra at lower tangent heights. Visual inspection showed that the reference spectra at tangent height steps 11 and 12 do not contain any OH Meinel emission features, as expected. Before the inversion the limb-radiances for the different OH bands are spectrally averaged over the spectral ranges listed in Table 1 to yield the elements of the measurement vectors $\boldsymbol{y}_{3-1}$, $\boldsymbol{y}_{6-2}$, and $\boldsymbol{y}_{8-3}$ that are inverted using Eq. (1). The maximum signal-to-noise ratios are on the order of 5000 for the OH(3-1) band, 50 for the OH(6-2) band and 10 for the OH(8-3) band.

4 Results

In order to allow for an easier comparison of the inverted volume emission rate profiles of the three OH-Meinel bands analyzed, the volume emission rate profiles are normalized relative to their respective peak value for the following discussions.

The normalized volume emission rate profiles for all three OH Meinel bands and for July 2005 are shown in Fig. 2 for 10° latitude bands between −30° S and 10° N. Despite some

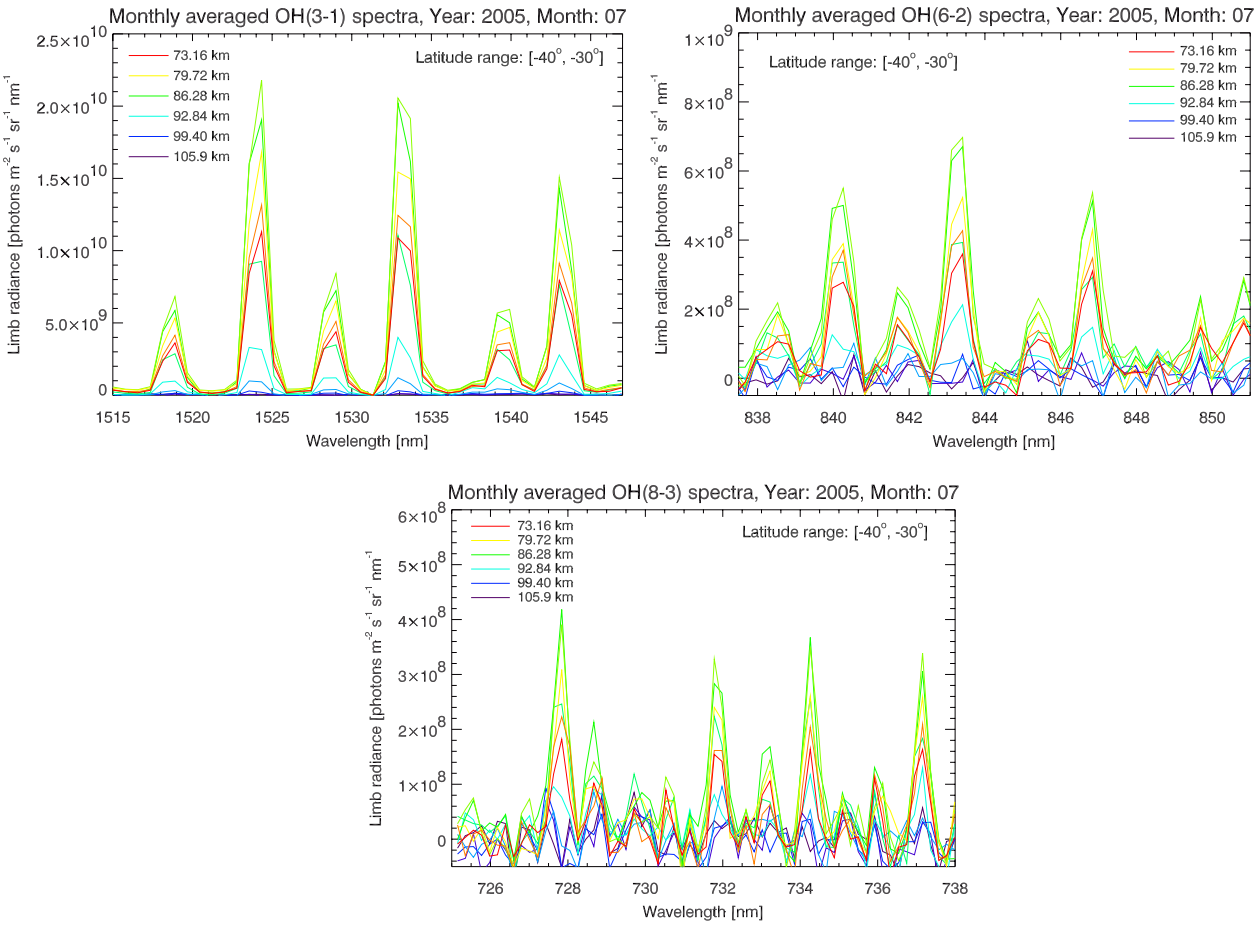

Fig. 1. Monthly and zonally averaged OH(3-1), OH(6-2) and OH(8-3) limb spectra for July 2005 and the 40° S–30° S latitude range. Note that the limb emission spectra at every second tangent height have been omitted for the sake of clarity.

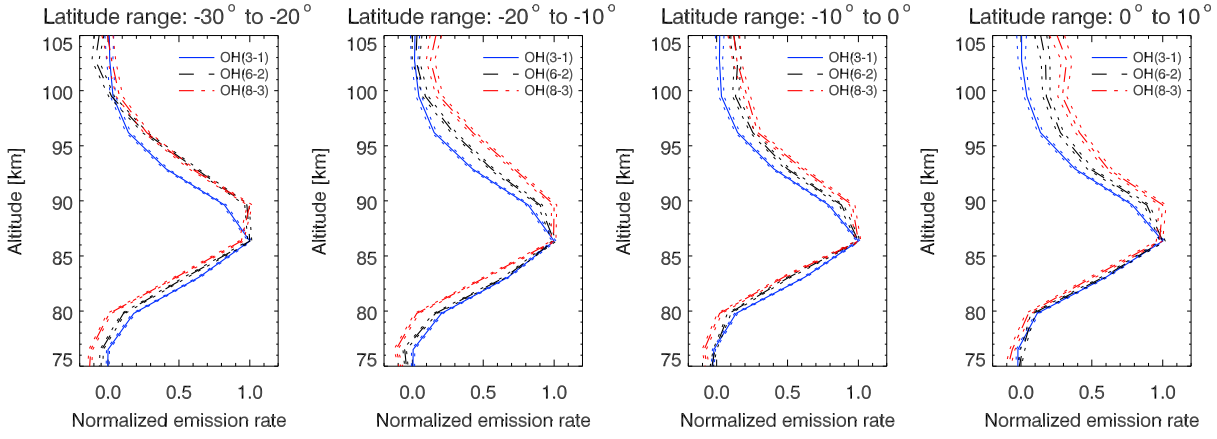

Fig. 2. Monthly and zonally averaged vertical volume emission rate profiles of the OH(3-1), OH(6-2) and OH(8-3) bands for 10° latitude bins between 30° S and 10° N and July 2005. The dotted lines indicate the retrieval errors based on the standard error of the inverted limb-radiance profiles.

Table 2. Compilation of rocket OH profile measurements listed in Table V of Baker and Stair (1988) that cover different OH Meinel bands simultaneously.

Code	Date	Reference	Location	Latitude	Longitude	Peak altitude [km]	OH Bands
720391	8 February 1972	Evans et al. (1973)	Churchill, MB, Canada	58.5° N	94° W	84.0	3-1–5-3
720392	8 February 1972	Evans et al. (1973)	Churchill, MB, Canada	58.5° N	94° W	84.0	3-1–5-3
720393	8 February 1972	Evans et al. (1973)	Churchill, MB, Canada	58.5° N	94° W	87.5	5-3–7-5
720394	8 February 1972	Evans et al. (1973)	Churchill, MB, Canada	58.5° N	94° W	88.0	5-3–7-5
720661	6 February 1972	Rogers et al. (1973)	White Sands, NM, US	32.5° N	107° W	82.0	3-1–5-3
720662	6 February 1972	Rogers et al. (1973)	White Sands, NM, US	32.5° N	107° W	84.0	7-5–8-6
731061	16 April 1973	Good (1976)	White Sands, NM, US	32.5° N	107° W	93.0	7-4–9-6
731062	16 April 1973	Good (1976)	White Sands, NM, US	32.5° N	107° W	87.0	3-1–6-4
732772	4 October 1973	Baker (1978)	White Sands, NM, US	32.5° N	107° W	87.0	4-2–5-3
732773	4 October 1973	Baker (1978)	White Sands, NM, US	32.5° N	107° W	89.2	7-5–8-6
750631	4 March 1975	Baker (1978)	Chatanika, AK, US	65.1° N	148° W	87.7	4-2–5-3
750632	4 March 1975	Baker (1978)	Chatanika, AK, US	65.1° N	148° W	89.0	7-5–8-6
771921	11 July 1977	Thomas and Young (1981)	White Sands, NM, US	32.5° N	107° W	88.0	5-3–6-4
771922	11 July 1977	Thomas and Young (1981)	White Sands, NM, US	32.5° N	107° W	87.0	5-3–6-4
771923	11 July 1977	Thomas and Young (1981)	White Sands, NM, US	32.5° N	107° W	87.0	7-4–9-6
771924	11 July 1977	Thomas and Young (1981)	White Sands, NM, US	32.5° N	107° W	89.0	7-4–9-6
813531	19 December 1981	López-Moreno et al. (1984)	Huelva, Spain	37.5° N	6.4° W	84.0	3-1–4-2
813532	19 December 1981	López-Moreno et al. (1984)	Huelva, Spain	37.5° N	6.4° W	87.5	4-2–5-3
813533	19 December 1981	López-Moreno et al. (1984)	Huelva, Spain	37.5° N	6.4° W	87.0	5-3–6-4
820821	23 February 1982	Greer et al. (1986)	South Uist, Scotland	57.4° N	7.4° W	92.5	8-3
820822	23 February 1982	Greer et al. (1986)	South Uist, Scotland	57.4° N	7.4° W	87.0	$\Delta\nu = 2$*

* The photometer had a center wavelength of 1610 nm and a bandwidth of 194 nm, i.e. covered the OH(5-3), OH(4-2) and OH(3-1) bands.

variability and despite the fact that SCIAMACHY is not able to identify the exact peak altitude – because of the ≈2.8 km vertical field of view and the 3.3 km tangent height sampling – it is evident that the OH(6-2) peak altitude is systematically higher than for the OH(3-1) band, and the OH(8-3) peak altitude is generally higher than for the OH(6-2) band. The total altitude shift – considering only altitudes above the emission maximum – between the OH(3-1) and the OH(8-3) profiles can be as large as 3–4 km. We also note the presence of an asymmetry with larger vertical shifts above the emission maximum and smaller shifts below. The origin of this apparent asymmetry will be discussed further and explained in section 5.

In order to check, whether the retrieval code is capable of reproducing the observed limb-radiance profiles we compare in Fig. 3 the observed limb-radiance profiles (blue solid lines) for the three Meinel bands with the forward-modelled profiles (solid black circles) based on the retrieved volume emission rate profiles. The measurement errors are indicated by the blue dotted lines. Evidently, the retrieval is able to reproduce the observed limb-radiance profiles well, which is an important consistency check.

Note that even in the original limb-radiance profiles the difference in peak altitude between the three OH Meinel bands is already evident. Fig. 4 shows the normalized (with respect to the maximum limb-radiance) limb-radiance profiles for the OH(3-1), OH(6-2) and OH(8-3) bands that were used for the inversion to vertical volume emission rate profiles shown in Fig. 2. As in the case of the inverted volume emission rate profiles there is – despite some variability – a fairly systematic vertical shift of the emitting layers with the bands originating from higher vibrational levels occurring at slightly higher altitudes. Again, the exact emission peak altitude differences cannot be resolved with SCIAMACHY due to the relatively large vertical field of view and the vertical sampling. However, the altitude shifts are evident.

The inversion algorithm was applied to the SCIAMACHY data set between September 2002 and December 2010. The results for all months in this period and for all latitude bins are very similar to the ones shown in Figs. 2 and 4 and clearly indicate that OH Meinel emissions originating from higher vibrational levels typically peak at slightly higher altitudes.

4.1 Comparison to previous results

We now discuss whether our findings are consistent with the results presented in the limited number of earlier observational studies on this topic. Comparisons with published and new model simulations will be presented and discussed in Sect. 5.

López-Moreno et al. (1987) retrieved vertical density profiles of OH in vibrational states $\nu' = 2$–7 from

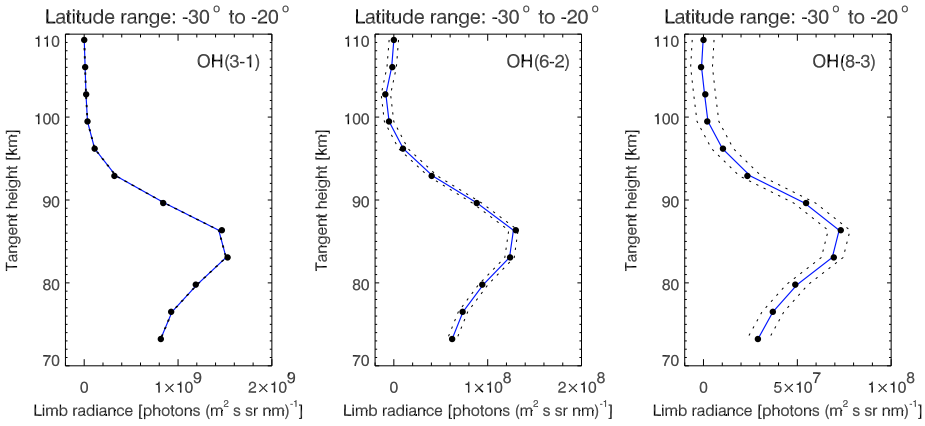

Fig. 3. Comparison of observed and forward modelled limb-radiance profiles – based on the retrieved volume emission rate profiles – for a sample latitude bin and the OH(3-1), OH(6-2) and the OH(8-3) bands. The observed limb-radiance profiles are shown as solid blue lines, the dotted lines indicate the measurement error. The solid black circles correspond to the forward modelled limb-radiance profiles.

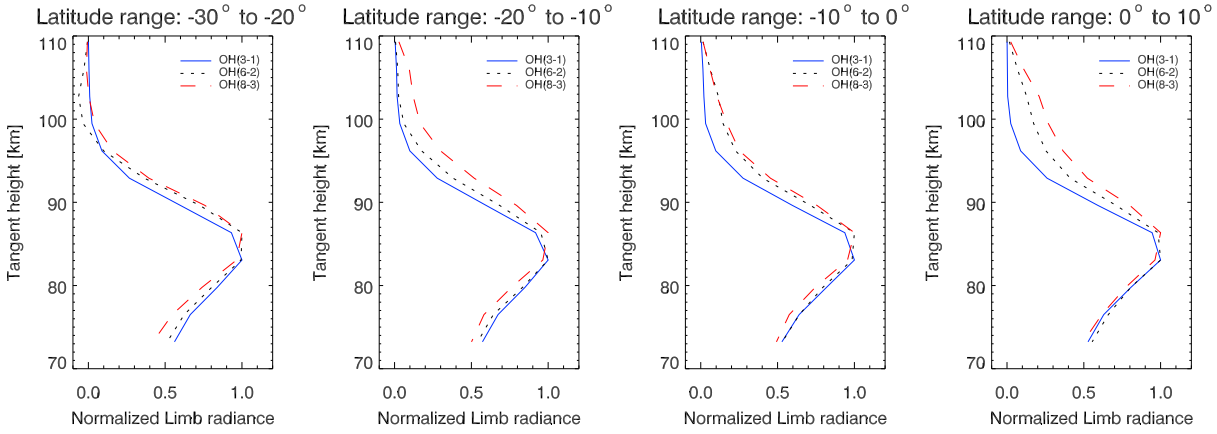

Fig. 4. Normalized monthly and zonally averaged limb-radiance profiles for the OH(3-1), OH(6-2) and the OH(8-3) band and the same latitude bins as in Fig. 2. The profiles are normalized with respect to the peak values for easier comparison. The altitude shifts between the different bands are already visible in the un-inverted limb-radiance profiles.

multi-band rocket photometer observations. Each of the three photometer passbands covered several OH Meinel transitions. López-Moreno et al. (1987) found a maximum peak altitude difference of about 5 km. Interestingly, the density peak altitude does not increase monotonously with increasing vibrational level. The largest density peak altitude was found for $\nu' = 5$ (about 91 km), and the peak altitudes for $\nu' = 6$ and 7 were again 3 km lower. The SCIAMACHY results presented here are only partly consistent with the results by López-Moreno et al. (1987) in the sense that significant differences in density peak altitude – and consequently emission peak altitude – are found for the different values of ν'. However, López-Moreno et al. (1987) do not find the largest emission peak altitude to be associated with the highest vibrational level, contradicting the results presented here.

One of the most important and most cited previous studies on the altitude of the OH Meinel emission bands was published by Baker and Stair (1988), providing a comprehensive compilation of rocket observations of OH emission rate profiles carried out between 1956 and 1984. Baker and Stair (1988) even explicitly discuss altitude differences between different upper vibrational states in the context of the USU/AFGL (Utah State University/Air Force Geophysics Laboratory) dual photometer rocket observations of the (4-2) and (5-3) as well as the (7-5) and (8-6) bands of OH (see Table IV in Baker and Stair, 1988, and Table 2 of this study). For the New Mexico observations in 1973 the emission peak altitude of the OH(4-2) and OH(5-3) bands is 87 km, whereas for the OH(7-5) and OH(8-6) bands a value of 89.2 km is found, i.e. roughly 2 km difference for a difference in vibrational levels of 3. For the Alaska observations in 1975 a peak altitude 87.7 km is found for the OH(4-2) and OH(5-3) bands, whereas 89.9 km was derived for the OH(7-5) and OH(8-6) bands. Baker and Stair (1988) treat these altitude

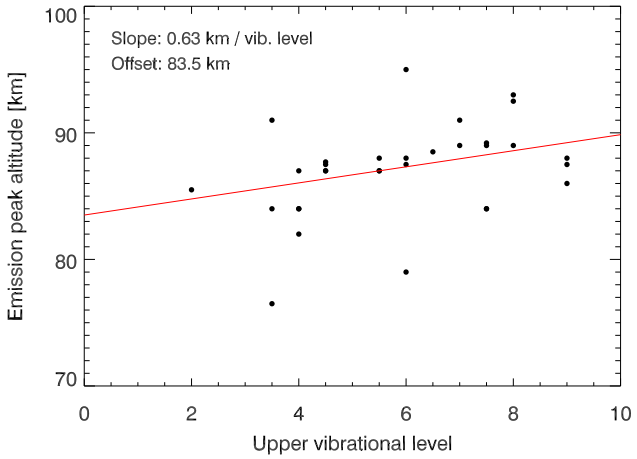

Fig. 5. Dependence of OH(ν', ν'') emission peak altitude on the upper vibrational level ν' as extracted from Table V in Baker and Stair (1988). See text for a detailed description of the data screening applied.

differences with caution due to potential contamination by the $O_2(^1\Delta_g)$ emission – although this emission does not overlap with any of the bands discussed – and possible effects caused by gravity waves.

We now investigate, whether the ν-dependence of the emission peak altitude observed in SCIAMACHY data is also present in the OH peak altitude observations compiled in Baker and Stair (1988) (their Table V). The Table lists results of 56 OH observations – mainly rocket observations, but also a few satellite measurements – carried out at different locations (latitudes vary between 3° S and 75° N) between July 1956 and February 1984. A few observations yielded emission peak thicknesses that may be considered unrealistically large and in the following observations with emission peak thicknesses exceeding 17 km are excluded (9 cases). Note that many studies measure several OH bands simultaneously. In those cases the mean upper vibrational level is determined and studies with filters covering bands originating from more than 3 adjacent vibrational levels are not considered. Fig. 5 shows for the remaining cases the dependence of the emission peak altitude listed in Table V of Baker and Stair (1988) on the upper vibrational level. Despite the scatter, Fig. 5 indicates that the emission peak altitude increases with increasing vibrational level. A linear fit to the set of data points shown in Fig. 5 yields a slope of 0.63 ± 0.30 km per vibrational level, which is in good quantitative agreement with the SCIAMACHY results presented in this study, as well as with the model simulations by Adler-Golden (1997) and the ones presented later in Sect. 5.

The above interpretation of the results by Baker and Stair (1988) may be criticized, because measurements at different latitudes and local times are combined, and possible latitude and tidal variations of the emission peak altitude may interfere with the dependence on the upper vibrational level. In order to eliminate these effects we now only focus on the observations listed in Table V of Baker and Stair (1988) that were carried out at the same location, on the same day and at the same time. Limiting the analysis to observations with emission peak widths smaller than 17 km, and to OH emissions originating from 3 or less adjacent vibrational levels leads to 8 cases of simultaneous observations of different Meinel bands. These measurements are listed in Table 2. For 6 out of these 8 cases, the OH emission profiles peak at higher altitudes for higher vibrational levels. The two exceptions are the measurements reported by Thomas and Young (1981) and by López-Moreno et al. (1984). The Thomas and Young (1981) measurements (codes 771921–771924) are partly inconsistent with the hypothesis that OH in higher vibrational levels emits at slightly higher altitudes. Two of these four measurements cover the OH (5-3) to (6-4) bands, and the remaining two the (7-4) to (9-6) bands. If the mean OH emission peak altitudes for the (5-3) to (6-4) bands and the (7-4) to (9-6) bands are compared, then the emission originating from the higher vibrational levels occurs at a higher altitude. Also, the 3 measurements by López-Moreno et al. (1984) are only partly consistent with the assumption that the emission from higher vibrational levels peaks at higher altitudes: the (3-1) to (4-2) bands peak at 84.0 km, the (4-2) to (5-3) bands at 87.5 (consistent with the hypothesis that emissions from higher vibrational levels peak at higher altitudes), but the (5-3) to (6-4) band peaks at 87.0 km.

For completeness we mention that Ulwick et al. (1986) (codes 840411 and 840412) also reported on simultaneous observations of OH emission rate profiles – of the same bands, however – and found a difference in peak altitude of 4 km.

The overall conclusion of the analysis of the observations compiled by Baker and Stair (1988) is that the majority of the coincident rocket measurements of different OH bands is consistent with the hypothesis, that emissions from higher vibrational levels peak at higher altitudes.

Mende et al. (1993) presented another study addressing the question, whether OH emissions from higher vibrational levels occur at higher altitudes. The authors used measurements taken with a grating spectrometer flown on the space shuttle (mission STS-37) in November 1990. The emission rate profiles of several OH Meinel bands were observed (8-3, 7-2, 6-1, 9-3, and 6-0), but no systematic dependence of the emission peak altitude with vibrational level was found.

In a more recent study Kaufmann et al. (2008) presented an example of limb-radiance profiles in the OH(9-6) and the OH(3-1) Meinel band – observed with SCIAMACHY – that suggests a vertical shift of the OH(9-6) relative to the OH(3-1) emission layer of about 3 km. This altitude shift is roughly consistent with about 0.5 km vertical displacement per vibrational level. However, the data presented by Kaufmann et al. (2008) is only an example and the presented, i.e. uninverted limb-radiance profiles do not allow accurate determination of the altitude shift.

Finally, it is noteworthy that differences in emission peak altitudes for different vibrational levels similar to the ones seen in the SCIAMACHY observations presented here were recently also identified in OSIRIS (Optical Spectrograph and InfraRed Imager System) (Llewellyn et al., 2004) observations (R. Gattinger, personal communication, 2011) as well as SABER (Sounding the Atmosphere using Broadband Emission Radiometry) (Russell et al., 1999) measurements (J.-H. Yee, personal communication, 2011; See also Xu et al. (2012)). In terms of OSIRIS observations vertical volume emission rate profiles of the OH(3-1) and OH(9-4) bands yielded vertical shifts of up to about 3 km with the OH(9-4) band peaking at higher altitudes (R. Gattinger, personal communication, 2011). SABER has broad-band channels near 1.6 μm and 2.0 μm covering the (5-3)/(4-2) and the (9-7)/(8-6) bands of OH, respectively. For tropical latitudes and July 2005, the SABER OH emission profile measurements show an altitude shift between the 2 channels of about 2 km, with the emission rate profile peak of the 2.0 μm channel occurring at a higher altitude (J.-H. Yee, personal communication, 2011). The recent study by Xu et al. (2012) also shows systematic vertical shifts – consistent with the other results discussed here – of the volume emission rate profiles retrieved from observations in the two SABER channels of 2–3 km for selected days of the year 2003. Note that all of these observations are approximately consistent with a 0.5 km altitude shift per vibrational level. A detailed comparison of the SCIAMACHY, SABER as well as OSIRIS results on vertical shifts between OH Meinel bands originating from different vibrational levels will be presented in a follow-up publication (McDade et al., 2012; to be submitted).

In conclusion, we note that – despite the existence of some contradicting cases – the majority of the previously published experimental studies are in fact consistent with the hypothesis, that the OH emissions originating from higher vibrational levels peak at higher altitudes.

5 Model simulations

The model employed here is based on the model also used by McDade (1991). As the model has been described in detail in McDade and Llewellyn (1987) and McDade (1991) only the most important features as well as the changes are described here. As mentioned above, the reaction

$$\mathrm{H} + \mathrm{O_3} \longrightarrow \mathrm{OH}(\nu' \leq 9) + \mathrm{O_2} \qquad k_1 \quad \text{(R2)}$$

is generally considered to be the only excitation mechanism of vibrationally excited OH near the mesopause, producing OH molecules preferentially in the $\nu = 6, 7, 8, 9$ vibrational levels. The lower vibrational states can be populated through a radiative cascade from the initially populated higher levels

$$\mathrm{OH}(\nu') \longrightarrow \mathrm{OH}(\nu'') + h\nu \qquad A(\nu', \nu'') \quad \text{(R3)}$$

or by collisional relaxation

$$\mathrm{OH}(\nu') + Q \longrightarrow \mathrm{OH}(\nu'') + Q \qquad k_3^Q(\nu', \nu'') \quad \text{(R4)}$$

with $Q = \mathrm{O_2}, \mathrm{N_2}$.

Additionally, vibrationally excited OH may be entirely removed:

$$\mathrm{OH}(\nu') + Q \longrightarrow \text{other products} \qquad k_4^Q(\nu') \quad \text{(R5)}$$

with $Q = \mathrm{O}, \mathrm{O_2}, \mathrm{N_2}$.

Following McDade (1991), the concentration of OH in vibrational state ν can be – for steady state conditions – expressed by:

$$[\mathrm{OH}(\nu)] = \left(A(\nu) + \sum_Q k_\mathrm{L}^Q(\nu)[Q] \right)^{-1} \times \left(p(\nu) + \sum_{\nu^*=\nu+1}^{9} [\mathrm{OH}(\nu^*)] \{ A(\nu^*, \nu) + \sum_Q k_3^Q(\nu^*, \nu)[Q] \} \right) \tag{3}$$

where $p(\nu)$ is the nascent production rate of OH in vibrational level ν, and k_L^Q is the total rate constant for removal of OH in vibrational level ν through Reactions (R4) and (R5). $A(\nu)$ corresponds to the inverse radiative lifetime of OH in vibrational level ν.

Equation (3) can be transformed into an expression for the relative population of vibrational level ν with respect to $\nu = 9$:

$$N(\nu) = \left(a(\nu) + K_L^{\mathrm{O_2,N_2}}(\nu)[\mathrm{O_2}] + K_\mathrm{L}^\mathrm{O}(\nu)[\mathrm{O}] \right)^{-1} \times \left(\begin{array}{c} F(\nu)\{1 + K_\mathrm{L}^{\mathrm{O_2,N_2}}(9)[\mathrm{O_2}] + K_\mathrm{L}^\mathrm{O}(9)[\mathrm{O}]\} + \\ \sum_{\nu^*=\nu+1}^{9} N(\nu^*)\{a(\nu^*, \nu) + K_3^{\mathrm{O_2,N_2}}(\nu^*, \nu)[\mathrm{O_2}]\} \end{array} \right) \tag{4}$$

Here, $F(\nu) = p(\nu)/p(9)$, $a(\nu^*, \nu) = A(\nu^*, \nu)/A(9)$ and the remaining quantities are defined as in McDade (1991). Equation (4) is in the following used to calculate the fractional population of OH for the different vibrational levels ν.

McDade (1991) determined the fractional population of the OH vibrational levels $\nu = 1, \ldots, 9$ based on 4 different sets of assumptions: a collisional cascade model without quenching by atomic oxygen, a sudden-death model without quenching by atomic oxygen, a collisional cascade model with maximum atomic oxygen quenching as well as a sudden death model with maximum quenching by atomic oxygen. The 4 sets of assumptions lead to differences in the modelled OH emission peak altitude associated with all vibrational levels of 1–2 km at most. The two models that ignore quenching by atomic oxygen cause vibrational bands originating from lower vibrational levels to peak at higher altitudes, contradicting the SCIAMACHY results presented in this study and also contradicting several earlier studies, as

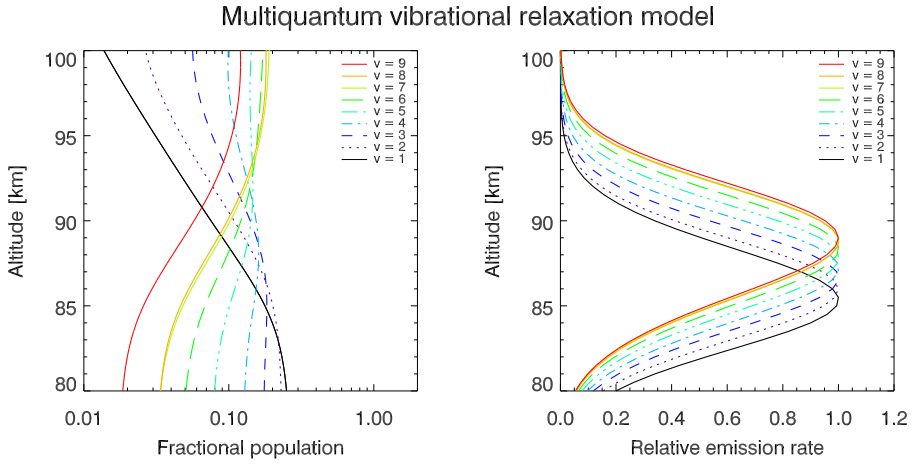

Fig. 6. Left panel: fractional populations of OH vibrational levels $v = 1, \ldots, 9$ as a function of altitude based on Eq. (4). The lifetime at level $v = 9$ ($A(9)^{-1}$) was taken from Langhoff et al. (1986), the nascent population by Steinfeld et al. (1987) (see Table 3) was used and O-quenching based on the rate constant in Adler-Golden (1997) was considered. Right panel: normalized emission rate profiles for vibrational levels $v = 1, \ldots, 9$ calculated with Eq. (7).

discussed in Sect. 4. Therefore, taking quenching by atomic oxygen into account appears to be a necessary prerequisite for reproducing a realistic dependence of the emission peak altitude on vibrational level. The importance of quenching by atomic oxygen was also emphasized in the model study by Makhlouf et al. (1995).

For the initial model simulations presented here the O-quenching rate constant also assumed by Adler-Golden (1997) was used, i.e. $k_L^O(v) = 2 \times 10^{-11}$ cm^3 s^{-1} for all vibrational levels v. Note that this value is very similar to the maximum O-quenching case of McDade (1991) – considering typical radiative lifetimes at vibrational level $v = 9$ – and it was also used in the study by Kaufmann et al. (2008). In Sect. 5.1 we also test the effect of using the O-quenching rate constant recently suggested by Smith et al. (2010) including the correction presented in Xu et al. (2012).

Following McDade (1991), the relative transition probabilities $A(v', v'')$ are taken from Murphy (1971), and $A(9)$ – the inverse lifetime of level $v = 9$ – is taken for test purposes from Mies (1974), Langhoff et al. (1986) or Turnbull and Lowe (1989), as described below. It is found, however, that the resulting relative populations of the vibrational levels as well as the modelled vertical emission rate profiles are very insensitive to the assumed value of $A(9)$. Vertical concentration profiles of O, O_2 and N_2 are taken from the MSIS-E90 climatology (Hedin, 1991).

The collisional cascade model used by McDade (1991) only allowed for single-quantum collisional deactivation. Following Adler-Golden (1997), the model by McDade (1991) was extended in the following way: multi-quantum collisional deactivation by O_2 is considered by using the state-to-state quenching rate constants listed in Table 3 of Adler-Golden (1997). Adler-Golden (1997) determined the rate constants for multi-quantum collisional relaxation empirically assuming an exponential scaling of the rate constants with quantum number difference Δv (Eq. 11 in Adler-Golden, 1997) using zenith observations of several Meinel bands reported by Takahashi and Batista (1981). For N_2 – an inefficient quencher of OH – single-quantum deactivation is assumed, and the v-dependent rate constants also used by Adler-Golden (1997) are adopted here.

This model is then used to determine the fractional population of the different vibrational levels as a function of altitude. The left panel of Fig. 6 shows the fractional population of the different vibrational states as a function of altitude determined with Eq. (4), assuming the nascent population by Steinfeld et al. (1987) (see Table 3). Evidently, the model produces a fairly significant altitude variation of the fractional population of the OH vibrational levels $v = 1, \ldots, 9$. The fractional population of the higher vibrational levels increases with increasing altitude. This altitude variation in fractional population is more pronounced than for any of the four cases investigated by McDade (1991).

In a next step the relative fractional populations are used to model the v-dependence of the OH emission rate profiles. This model is based on the following assumptions:

1. The initially produced OH* follows a Gaussian altitude profile with a peak height of $z^{\text{mean}} = 87$ km, and a FWHM of 8 km, based on the results of Baker and Stair (1988):

$$G(z) = \frac{1}{\sqrt{2\pi}\sigma} \exp\left(-\frac{(z - z^{\text{mean}})^2}{2\sigma^2}\right) \quad (5)$$

with $\sigma = \frac{\text{FWHM}/2}{\sqrt{2\ln 2}}$.

Table 3. Nascent vibrational level distributions used for model simulations.

	Ohoyama et al. (1985)*	Steinfeld (1987)**
$p(9)$	0.32	0.47
$p(8)$	0.29	0.34
$p(7)$	0.19	0.15
$p(6)$	0.06	0.03
$p(5)$	0.06	0.01
$p(4)$	0.06	0.00
$p(3)$	0.06	0.00
$p(2)$	0.00	0.00
$p(1)$	0.00	0.00

* Adjusted as described in McDade (1991).
** Adjusted as described in Adler-Golden (1997).

2. The resulting vertical emission rate profile $\mathrm{VER}(\nu, z)$ associated with emission from vibrational level ν is now determined by weighting $G(z)$ with the fractional population $\mathrm{N}(\nu)$ (see Eq. 4):

$$\mathrm{VER}(\nu, z) = \mathrm{N}(\nu) \times G(z) \quad (6)$$

3. For easier comparison of the volume emission rate profiles for different vibrational levels ν the emission rate profile of every ν is normalized to its maximum value, i.e. the peak values of the normalized emission rate profiles for different ν are all 1:

$$\mathrm{VER}_n(\nu, z) = \frac{\mathrm{VER}(\nu, z)}{\mathrm{MAX}(\mathrm{VER}(\nu, z))} \quad (7)$$

The resulting normalized volume emission rate profiles associated with the different upper vibrational levels $\nu = 1, \ldots, 9$ are shown in the right panel of Fig. 6. As this figure illustrates, the pronounced altitude variation in fractional population (left panel of the same figure) also leads to significant differences in the normalized emission rate peak altitudes for the different vibrational levels, with emissions originating from lower vibrational levels occurring at lower altitudes. The peak altitude difference between the vibrational levels $\nu = 1$ and $\nu = 9$ is about 4 km, leading to an averaged peak altitude difference of about 0.5 km for emissions originating from adjacent vibrational levels. This altitude difference for adjacent vibrational levels is – as expected – consistent with Adler-Golden (1997). A closer inspection of the right panel of Fig. 6 shows that the emission peaks are not equally spaced in altitude. The peak altitude difference between adjacent vibrational levels decreases with increasing vibrational level.

Based on (a) the model simulations performed here, and (b) the differences between our model results and the ones reported in McDade (1991) we conclude that both quenching by atomic oxygen as well as multi-quantum collisional relaxation by O_2 are important in terms of reproducing the observed vibrational level dependence of the OH emission peak altitude. In order to evaluate the relative contributions of O-quenching and the multi-step quenching by O_2 to the strong vibrational level dependence in OH emission peak altitude seen in Fig. 6, we ran the model in a separate test without any quenching by atomic oxygen. The results of this test are presented in Fig. 7. The altitude dependence of the fractional population is significantly smaller if quenching by atomic oxygen is not considered. It is worth noting that for altitudes between 80 and 85 km the modelled fractional populations for the two cases (with and without O-quenching) are very similar. This effect is easily explained by the strong increase in [O] with increasing altitude in combination with the decreasing concentrations of O_2 and N_2 with increasing altitude, which make quenching by O a relatively inefficient process below 85 km. At higher altitudes the lower vibrational levels are more strongly quenched by O than by O_2 – relative to lower altitudes – which leads to the decreasing fractional populations of the lower vibrational states at altitudes above about 85 km in the left panel of Fig. 6. In terms of the vibrational level dependence of the volume emission rate profiles, neglecting quenching by O leads to a significantly reduced ν-dependence of the emission peak altitude (compare right panels of Figs. 7 and 6). However, in contrast to the findings of McDade (1991), neglecting O-atom quenching leads to the correct ν-dependence of the emission peak altitude in a qualitative sense (except for $\nu' = 9$), i.e. emissions originating from higher vibrational levels peak at higher altitudes. This finding again confirms that both, quenching by atomic oxygen as well as multi-quantum collisional deactivation contribute to the vibrational level dependence of the emission peak altitude.

5.1 Sensitivity tests

In order to investigate the sensitivity of the model results to some of the basic assumptions made we performed a series of tests. Note that a more comprehensive sensitivity study treating effects of uncertainties in all parameters and testing all published rate constants available for the relevant reactions is beyond the scope of this study.

5.1.1 Rate constants for quenching by O and O_2

The analysis presented above indicates that quenching by atomic oxygen is the key process to explain the vertical shifts between Meinel emissions originating from different vibrational levels. Accurate modelling of this quenching requires accurate knowledge of the atomic oxygen concentration profile in the MLT region as well as of the reaction rates for both quenching by O (Reaction R5) and collisional relaxation by O_2 (Reaction R4). Particularly the O-quenching reaction rate is uncertain (see Table 4 in Xu et al. (2012) for a compilation of published rate constants) and in order to test the sensitivity

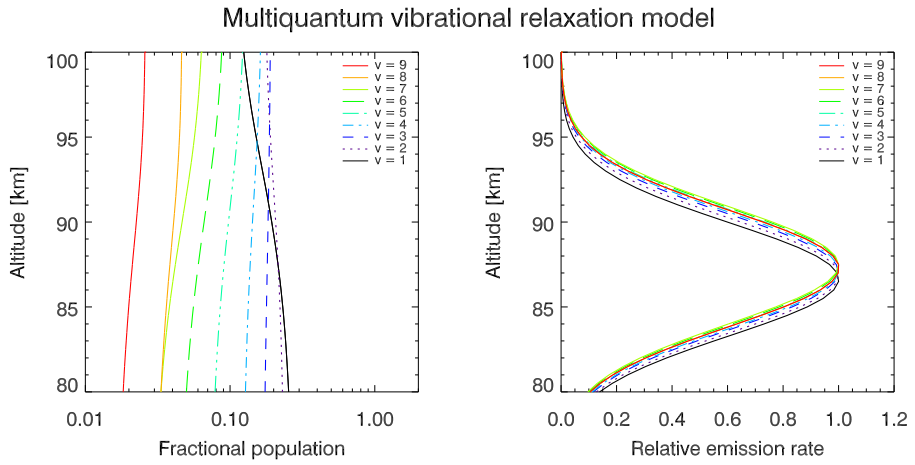

Fig. 7. Fractional population of different vibrational levels (left panel) and modelled vertical emission rate profiles (right panels) for the same parameters as in Fig. 6, except that quenching by atomic oxygen is entirely neglected.

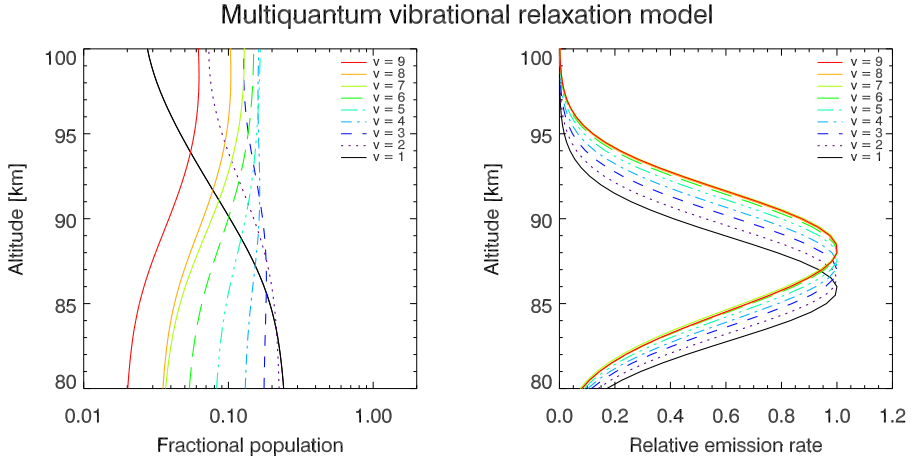

Fig. 8. Same as in Fig. 6, except that quenching by atomic oxygen is modelled using the O-quenching rate constant taken from Smith et al. (2010) in combination with the correction factor ($\beta = 1.293$) from Xu et al. (2012). Adjusted O_2-quenching is also taken from Xu et al. (2012), but is found to have only minor impact on the model results.

of the results to the value of the O-quenching rate we use the recently published rate constant value by Smith et al. (2010) in combination with the correction factor ($\beta = 1.293$) derived by Xu et al. (2012). The Smith et al. (2010) value is with $k_L^O(v) = 0.5 \times 10^{-11}\,cm^3\,s^{-1}$ only one forth of the Adler-Golden (1997) value. Based on the case study neglecting quenching by atomic oxygen described above, we expect that the vertical shifts between emissions from different vibrational levels will be smaller with the Smith et al. (2010) value compared to the Adler-Golden (1997) value. Figure 8 demonstrates that this is the case, showing the model results including the Smith et al. (2010)/Xu et al. (2012) value as well as the Xu et al. (2012) correction of the O_2 quenching rate constant. Note that the effect of the O_2 quenching rate constant correction on the model results is only minor. Figure 8 also demonstrates, that the asymmetry in terms of smaller vertical shifts below the emission peak and larger shifts above the emission peak is now more pronounced, in agreement with the SCIAMACHY results presented in Fig. 2. We conclude that using the Smith et al. (2010) O-quenching rate constant including the Xu et al. (2012) correction factor ($\beta = 1.293$) allows for a more realistic modelling of the asymmetry seen in the SCIAMACHY measurements. We also tested using the Smith et al. (2010) O-quenching rate constant without applying the Xu et al. (2012) correction factor, and found that the effect of the Xu et al. (2012) correction factor is rather small, as expected.

5.1.2 Scaling the atomic oxygen concentration profile

In an additional test we investigated the sensitivity of the model results to changes in the atomic oxygen profile by

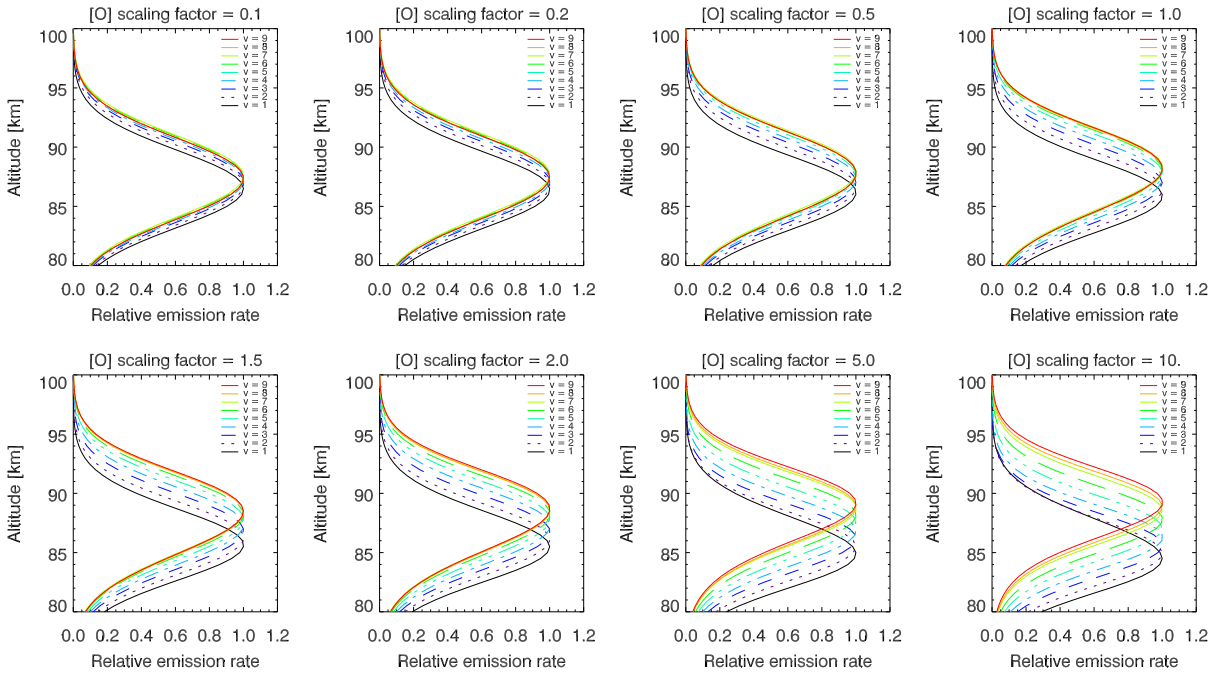

Fig. 9. Sensitivity of the modelled vertical emission rate profiles to the atomic oxygen profile. The standard MSIS atomic oxygen profile is scaled with constant factors varying between 0.1 (top left panel) and 10 (bottom right panel). The rate constants for quenching by atomic oxygen and molecular oxygen are the corrected values published in Xu et al. (2012).

scaling the atomic oxygen concentrations at all altitudes with a constant factor (ranging from 0.1 to 10) leaving all other parameters unchanged. The tests are performed with the Xu et al. (2012) values of the O and O_2 quenching rate constants. The resulting model output is displayed in Fig. 9. The main effect is an increase of the vertical shifts between emissions from different vibrational levels with increasing scaling factor. The results also demonstrate that the asymmetry discussed above – smaller/larger vertical shifts below/above the emission peak – becomes smaller again with increasing scaling factor if the factor exceeds a value of about 2. This may again suggests that the O-quenching rate constant employed by Adler-Golden (1997) is likely too large.

5.1.3 Variability of width and mean altitude of initially produced OH profile

The effect of changing the peak altitude and peak width of the initially produced OH^* (via the reaction $H + O_3 \longrightarrow OH^* + O_2$) on the model results was also investigated. For this purpose the mean altitude of the assumed Gaussian function was changed by $\pm$ 3 km and the FWHM was varied from 4 km to 12 km in steps of 2 km. The effect of changing the peak altitude is illustrated in the top row of Fig. 10 and the effect of changing the peak width is shown in the bottom row of this Figure. In terms of the peak altitude dependence of the model results the main conclusion of this study – emissions from higher vibrational levels peak at higher altitudes – is not affected. However, an increase in the vertical shifts is observed both below and above the emission peaks if the peak altitude becomes larger. This effect is again directly caused by the larger atomic oxygen concentrations at higher altitudes.

Regarding the effect of the peak width of the initially produced OH^* we find that the resulting vertical shifts are significantly affected (bottom panel of Fig. 10). The vertical shift increases with increasing peak width, and so does the asymmetry of the modelled emission rate profile. The latter effect is caused by the increasing difference in the atomic oxygen abundance – between altitudes in the lower and upper parts of the emission rate profile – for increasing peak width.

5.1.4 Effect of assumed nascent distribution and A(9)

Finally, we also tested the effect of the assumed nascent distribution $p(v)$ and the assumed value for the inverse radiative lifetime A(9) of level $v = 9$ on the fractional populations. The different nascent OH(v) distribution parameter sets used here are listed in Table 3. In terms of A(9) the values by Mies (1974), Turnbull and Lowe (1989) and Langhoff et al. (1986) were used. The differences in fractional populations and vertical emission rate profiles between the sets of nascent distributions and A(9) values were found to be very small (not shown).

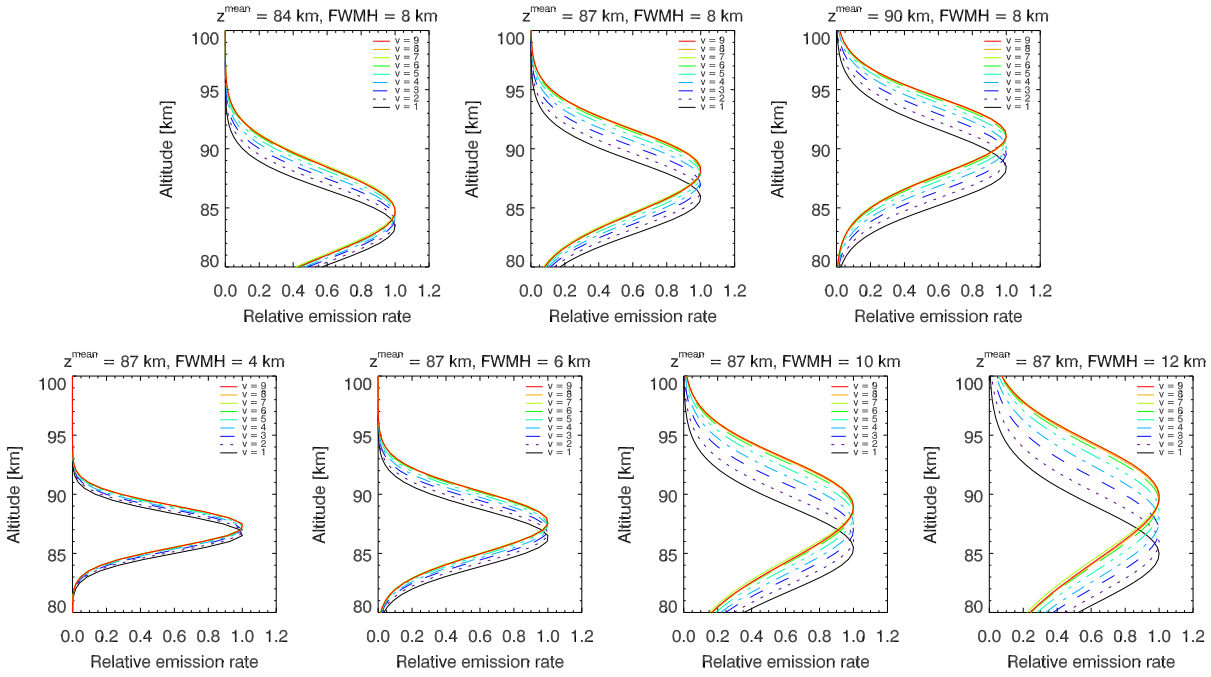

Fig. 10. Sensitivity of the modelled vertical emission rate profiles to peak altitude (top row) and peak width (bottom) of the initially produced OH* profile. The initially produced profile is assumed to follow a Gaussian function with peak altitude z^{mean} and a given FWHM. The rate constants for quenching by atomic oxygen and molecular oxygen are the corrected values published in Xu et al. (2012).

5.2 Comparison of SCIAMACHY observations and model results

We now discuss how the modelled differences in emission peak altitudes compare to the experimental results obtained from SCIAMACHY observations described above. In terms of the model results we focus on the simulations including the Xu et al. (2012) O and O_2 quenching rates (see Fig. 8), because those produce an asymmetry in terms of vertical shifts below and above the emission peak that is in better agreement with the SCIAMACHY observations. The modelled altitude difference between emissions from vibrational levels $\nu' = 6$ and $\nu' = 3$ is about1.0–1.5 km. This is in good quantitative agreement with the SCIAMACHY results indicating about a 1.0–2.0 km difference in emission altitude between these vibrational levels. The modelled altitude difference between vibrational levels $\nu' = 8$ and $\nu' = 6$ is with about 0.2 km significantly smaller than the observed difference of about 1 km. The reasons for this discrepancy are not fully known, but are likely related to the remaining uncertainty of the O-quenching rate constant and/or errors in the assumed atomic oxygen profile. Still, the model qualitatively reproduces the observed peak altitude differences.

6 Effect on ground-based OH temperature observations

In this section we briefly discuss the effect of different peak emission altitudes associated with OH Meinel emissions from different vibrational levels on OH temperature retrievals using ground-based observations. Note that a comprehensive investigation of these effects including consideration of, e.g. seasonal and latitudinal variations of the atmospheric temperature profile as well as possible variations in peak emission altitudes – and emission altitude differences for different vibrational levels – is beyond the scope of this study. Here we assume that the OH emission profile can be modelled with a Gaussian function with 8 km FWHM and different peak altitudes (z^{mean} in Eq. 5) and we use this function as a weighting function for the temperature profile. The temperature profile assumed was determined using the MSIS-90E model for 1 July 2005, a latitude of 0° and a longitude of 0°. The peak altitudes were then varied from 85 km to 89 km in steps of 0.5 km. The resulting difference in altitude-weighted temperature for a 4 km difference in emission peak altitude is 5.8 K, and the mean temperature difference for an emission peak difference of 0.5 km was found to be 0.65 K. If we assume that the emission peak of the OH(6-2) band may be 2 km higher than for the OH(3-1) band, then the resulting temperature difference between OH(6-2) and OH(3-1) measurements from the ground may be as large as about 2.6 K – ignoring all other potential difficulties associated with the comparison.

The exact numerical values of the temperature differences resulting from different emission peak altitudes will vary with season and latitude, but this simple analysis shows that the effect of different vibrational levels having different emission peak altitudes may cause differences between ground-based observations employing different OH Meinel bands on the order of a few K. Moreover, the analysis indicates that accurate knowledge on the OH emission peak altitude, peak width and its shape are essential for interpreting variations – particularly slow and long-term variations – in OH rotational temperature measurements from the ground. Available satellite observations of the OH emission layer, e.g. from SCIAMACHY or SABER should be used to complement ground-based OH rotational temperature measurements.

7 Conclusions

Vertical emission rate profiles of the OH(3-1), OH(6-2) and OH(8-3) Meinel emission bands in the terrestrial nightglow were retrieved from limb observations with SCIAMACHY on Envisat. The main focus of this study was to investigate, whether the emission peak altitudes of these three Meinel bands differ. Differences in emission peak altitude of up to 4 km between the OH(3-1) and the OH(8-3) bands were identified in the SCIAMACHY data set, with emissions originating from higher vibrational levels occurring at larger altitudes. The OH(6-2) emission rate profile is typically vertically shifted upward by 1–2 km relative to the OH(3-1) band, and the OH(8-3) band is generally found to peak about 1 km higher than the OH(6-2) band. A review of the existing studies addressing this issue revealed that the SCIAMACHY observations are consistent with the majority of the previously published results.

The SCIAMACHY observations were complemented by model simulations using an extended version of the McDade (1991) model that allows the relative population of the different vibrational levels of OH to be simulated. Although several of the assumed rate constants are still highly uncertain, the model simulations quantitatively reproduce the observed differences in emission peak altitudes between different vibrational levels. The emission peak altitudes of OH emissions from adjacent vibrational levels were found to differ by roughly 0.5 km. More comprehensive model simulations and comparisons of absolute emission rates are planned for the near future in order to investigate the possibility to empirically constrain the values of some of the relevant reaction rates.

Acknowledgements. This work was supported by the German Ministry of Education and Research (BMBF), the German aerospace center (DLR) and the University of Bremen, Germany. ICMcD acknowledges support from the Canadian Natural Science and Engineering Research Council (NSERC) and York University. SCIAMACHY is jointly funded by Germany, the Netherlands and Belgium.

Edited by: W. Ward

References

Adler-Golden, S.: Kinetic parameters for OH nightglow modeling consistent with recent laboratory measurements, J. Geophys. Res., 102, 19969–19976, 1997.

Baker, D. J.: AFGL-TR-78-0251, Air Force Geophysics Laboratories, Hanscom AFB, MA, 40, 1 January, 1978.

Baker, D. J. and Stair Jr., A. T.: Rocket measurements of the altitude distribution of the hydroxyl airglow, Phys. Scripta, 37, 611–622, 1988.

Baker, D. J., Thurgood, B. K., Harrison, W. K., Mlynczak, M. G., and Russell, J. M.: Equatorial enhancement of the nighttime OH mesospheric infrared airglow, Phys. Scr., 75, 615–619, doi:10.1088/0031-8949/75/5/004, 2007.

Bittner, M., Offermann, D., Graef, H.-H., Donner, M., and Hamilton, K.: An 18-year time series of OH rotational temperatures and middle atmosphere decadal variations, J. Atmos. Sol.-Terr. Phys., 64, 1147–1166, 2002.

Bovensmann, H., Burrows, J. P., Buchwitz, M., Frerick, J., Noël, S., Rozanov, V. V., Chance, K. V., and Goede, A. P. H.: SCIAMACHY: Mission objectives and measurement modes, J. Atmos. Sci., 56, 127–150, 1999.

Bramstedt, K., Noël, S., Bovensmann, H., Gottwald, M., and Burrows, J. P.: Precise pointing knowledge for SCIAMACHY solar occultation measurements, Atmos. Meas. Tech. Discuss., 5, 3797–3835, doi:10.5194/amtd-5-3797-2012, 2012.

Burrows, J. P., Hölzle, E., Goede, A. P. H., Visser, H., and Fricke, W.: SCIAMACHY – Scanning imaging absorption spectrometer for atmospheric chartography, Acta Astronaut., 35, 445–451, 1995.

Cosby, P. C. and Slanger, T. G.: OH spectroscopy and chemistry investigated with astronomical sky spectra, Can. J. Phys., 85, 77–99, 2007.

Dyrland, M. E., Mulligan, F. J., Hall, C. M., Sigernes, F., Tsutsumi, M., and Deehr, C. S.: Response of OH airglow temperatures to neutral air dynamics at 78° N, 16° E during the anomalous 2003–2004 winter, J. Geophys. Res., 115, D07103, doi:10.1029/2009JD012726, 2010.

Espy, P. J. and Stegman, J.: Trends and variability of mesospheric temperature at high latitudes, Phys. Chem. Earth, 27, 543–553, 2002.

Evans, W. F. J., Llewellyn, E. J., and Vallance Jones, A.: Altitude distribution of hydroxyl bands of the $\Delta V = 2$ sequence in the nightglow, Can. J. Phys., 51, 1288–1292, doi:10.1139/p73-170, 1973.

French, W. J. R. and Mulligan, F. J.: Stability of temperatures from TIMED/SABER v1.07 (2002–2009) and Aura/MLS v2.2 (2004–2009) compared with OH(6-2) temperatures observed at Davis Station, Antarctica, Atmos. Chem. Phys., 10, 11439–11446, doi:10.5194/acp-10-11439-2010, 2010.

Gao, H., Xu, J. Y., Chen, G. M., Yuan, W., and Beletsky, A. B.: Global distributions of OH and O2 (1.27 μm) nightglow emissions observed by TIMED satellite, Sci. China Tech. Sci., 54, 447–456, doi:10.1007/s11431-010-4236-5, 2011.

Good, R. E.: Determination of atomic oxygen density from rocket borne measurement of hydroxyl airglow, Planet. Space Sci. 24, 389–395, 1976.

Gottwald, M., Krieg, E., von Savigny, C., Noël, S., Bovensmann, H., and Bramstedt, K.: Determination of SCIAMACHY Line of Sight Misalignments, Proceedings of the Envisat Atmospheric Science Conference, ESA SP-636, Montreux, Switzerland, 23–27 April, 2007.

Greer, R. G. H., Murtagh, D. P., McDade, I. C., Dickinson, P. H. G., Thomas, L., Jenkins, D. B., Stegman, J., Llewellyn, E. J., Witt, G., Mackinnon, D. J., and Williams, E. R.: ETON 1: A data base pertinent to the study of energy transfer in the oxygen nightglow, Planet. Space Sci., 34, 771–788, 1986.

Hedin, A. E.: Extension of the MSIS Thermospheric Model into the Middle and Lower Atmosphere, J. Geophys. Res., 96, 1159–1172, doi:10.1029/90JA02125, 1991.

Heppner, J. P. and Meredith, L. H.: Nightglow emission altitudes from rocket measurements, J. Geophys. Res., 63, 51–65, 1958.

Kaiser, J., von Savigny, C., Eichmann, K.-U., Noël, S., Bovensmann, H., Frerick, J., and Burrows, J. P.: Satellite Pointing Retrieval from Solar UV-B Radiation Scattered in the Atmosphere by the Earth's limb, Can. J. Phys., 82, 1041–1052, 2004.

Kaufmann, M., Lehmann, C., Hoffmann, L., Funke, B., López-Puertas, M., von Savigny, C., and Riese, M.: Chemical heating rates derived from SCIAMACHY vibrationally excited OH limb emission spectra, Adv. Space Res., 41, 1914–1920, 2008.

Langhoff, S. R., Werner, H.-J., and Rosmus, P.: Theoretical transition probabilities for the OH Meinel system, J. Mol. Spectrosc., 118, 507–529, doi:10.1016/0022-2852(86)90186-4, 1986.

Liu, G. and Shepherd, G. G.: An empirical model for the altitude of the OH nightglow emission, Geophys. Res. Lett., 33, L09805, doi:10.1029/2005GL025297, 2006.

Llewellyn, E. J., Lloyd, N. D., Degenstein, D. A., Gattinger, R. L., Petelina, S. V., Bourassa, A. E., Wiensz, J. T., Ivanov, E. V., McDade, I. C., Solheim, B. H., McConnell, J. C., Haley, C. S., von Savigny, C., Sioris, C. E., McLinden, C. A., Griffioen, E., Kaminski, J., Evans, W. F. J., Puckrin, E., Strong, K., Wehrle, V., Hum, R. H., Kendall, D. J. W., Matsushita, J., Murtagh, D. P., Brohede, S., Stegman, J., Witt, G., Barnes, G., Payne, W. F., Piche, L., Smith, K., Warshaw, G., Deslauniers, D.-L., Marchand, P., Richardson, E. H., King, R. A., Wevers, I., McCreath, W., Kyrölä, E., Oikarinen, L., Leppelmeier, G. W., Auvinen, H., Mégie, G., Hauchecorne, A., Lefevre, F., de La Nöe, J., Ricaud, P., Frisk, U., Sjoberg, F., von Scheele, F., and Nordh, L.: The OSIRIS instrument on the Odin satellite, Can. J. Phys., 82, 411–422, doi:10.1139/P04-005, 2004.

López-Moreno, J. J., Vidal, S., Rodrigo, R., and Llewellyn, E. J.: Rocket borne photometric measurements of $O_2(^1\Delta_g)$, green line and OH Meinel bands in the nightglow, Ann. Geophys, 2, 61–66, 1984.

López-Moreno, J. J., Rodrigo, R., Moreno, F., López-Puertas, M., and Molina, A.: Altitude distribution of vibrationally excited states of hydroxyl at levels $\nu = 2$ to $\nu = 7$, Planet. Space Sci., 35, 1029–1038, 1987.

Makhlouf, U. B., Picard, R. H., and Winick, J. R.: Photochemical-dynamical modeling of the measured response of airglow to gravity waves: 1. Basic model for OH airglow, J. Geophys. Res., 100, 11289–11311, doi:10.1029/94JD03327, 1995.

Marsh, D. R., Smith, A. K., Mlynczak, M. G., and Russell III, J. M.: SABER observations of the OH Meinel airglow variability near the mesopause, J. Geophys. Res., 111, A10S05, doi:10.1029/2005JA011451, 2006.

McDade, I. C.: The altitude dependence of the OH($X^2\Pi$) vibrational distribution in the nightglow: some model expectations, Planet. Space Sci., 39, 1049–1057, 1991.

McDade, I. C. and Llewellyn, E. J.: Kinetic Parameters Related to Sources and Sinks of Vibrationally Excited OH in the Nightglow, J. Geophys. Res., 92, 7643–7650, 1987.

Meinel, A. B.: OH Emission Bands in the Spectrum of the Night Sky. II, Astroph. J., 112, p. 120, doi:10.1086/145321, 1950.

Mende, S. B., Swenson, G. R., Geller, S. P., Viereck, R. A., Murad, E., and Pike, C. P.: Limb View Spectrum of the Earth's Airglow, J. Geophys. Res., 98, 19117–19125, 1993.

Mies, F. H.: Calculated vibrational transition probabilities of OH($X^2\Pi$), J. Mol. Spectrosc., 53, 150–188, doi:10.1016/0022-2852(74)90125-8, 1974.

Murphy, R. E.: Infrared emission of OH in the fundamental and first overtone bands, J. Chem. Phys., 54, 4852–4959, doi:10.1063/1.1674762, 1971.

Ohoyama, H., Kasai, T., Yoshimura, Y., Kimura, H., and Kuwata, K.: Initial distribution of vibration of the OH radicals in the $H + O_3 \rightarrow OH(X^2\Pi) + O_2$ reaction, Chem. Phys. Lett., 118, 263–266, doi:10.1016/0009-2614(85)85312-4, 1985.

Reisin, E. R. and Scheer, J.: Searching for trends in mesopause region airglow intensities and temperatures at El Leoncito, Phys. Chem. Earth, 27, 563–569, 2002.

Rogers, J. W., Murphy, R. E., Stair Jr., A. T., Ulwick, J. C., Baker, K. D., and Jensen, L. L.: Rocket-borne Radiometric Measurements of OH in the Auroral Zone, J. Geophys. Res., 78, 7023–7031, 1973.

Russell III, J. M., Mlynczak, M. G., Gordley, L. L., Tansock, J. J., and Esplin, R. W.: An Overview of the SABER Experiment and Preliminary Calibration Results, Proc. SPIE, 3756, 277–288, 1999.

Sigernes, F., Shumilov, N., Deehr, C. S., Nielsen, K. P., Svenøe, T., and Havnes, O.: Hydroxyl rotational temperature record from the auroral station in Adventdalen, Svalbard (78° N, 15° E), J. Geophys. Res., 108, 1342, doi:10.1029/2001JA009023, 2003.

Smith, A. K., Marsh, D. R., Mlynczak, M. G. and Mast, J. C.: Temporal variations of atomic oxygen in the upper mesosphere from SABER, J. Geophys. Res., 115, D18309, doi:10.1029/2009JD013434, 2010.

Steinfeld, J. I., Adler-Golden, S. M., and Gallagher, J. W.: Critical survey of data on the spectroscopy and kinetics of ozone in the mesosphere and thermosphere, J. Phys. Chem. Ref. Data, 16, 911, 41 pp., 1987.

Takahashi, H. and Batista, P. P.: Simultaneous measurements of OH(9,4), (8,3), (7,2), (6,2), and (5,1) Bands in the Nightglow, J. Geophys. Res., 86, 5632–5642, doi:10.1029/JA086iA07p05632, 1981.

Thomas, R. J. and Young, R. A.: Measurement of Atomic Oxygen and Related Airglows in the Lower Thermosphere, J. Geophys. Res., 86, 7389–7393, 1981.

Turnbull, D. N. and Lowe, R. P.: New hydroxyl transition probabilities and their importance in airglow studies, Planet. Space Sci., 37, 723–738, doi:10.1016/0032-0633(89)90042-1, 1989.

Ulwick, J. C., Baker, K. D., Baker, D. J., Steed, A. J., and Pendleton Jr., W. R.: Mesospheric minor species determinations from rocket and ground-based i.r. measurements, J. Atmos. Terr. Phys, 49, 855–862, doi:10.1016/0021-9169(87)90024-9, 1986.

von Savigny, C., Eichmann, K.-U., Llewellyn, E. J., Bovensmann, H., Burrows, J. P., Bittner, M., Höppner, K., Offermann, D., Taylor, M. J., Cheng, Y., Steinbrecht, W., Winkler, P.: First near-global retrieval of OH rotational temperatures from satellite-based Meinel band emission measurements, Geophys. Res. Lett., 31, L15111, doi:10.1029/2004GL020410, 2004.

von Savigny, C., Kaiser, J. W., Bovensmann, H., Burrows, J. P., McDermid, I. S., and Leblanc, T.: Spatial and temporal characterization of SCIAMACHY limb pointing errors during the first three years of the mission, Atmos. Chem. Phys., 5, 2593–2602, doi:10.5194/acp-5-2593-2005, 2005.

Ward, W. E.: A simple model of diurnal variations in the mesospheric oxygen nightglow, Geophys. Res. Lett., 26, 3565–3568, doi:10.1029/1999GL003661, 1999.

Xu, J., Gao, H., Smith, A. K., and Zhu, Y.: Using TIMED/SABER nightglow observations to investigate hydroxyl emission mechanisms in the mesopause region, J. Geophys. Res., 117, D02301, doi:10.1029/2011JD016342, 2012.

Yee, J. H., Crowley, G., Roble, R. G., Skinner, W. R., Burrage, M. D., and Hays, P. B.: Global simulations and observations of O(1S), O2(1P) and OH mesospheric nightglow emissions, J. Geophys. Res., 102, 19949–19968, 1997.